The Astrophysical Journal, 641:547–555, 2006 April 10
© 2006. The American Astronomical Society. All rights reserved. Printed in U.S.A.

KECK INTERFEROMETER OBSERVATIONS OF FU ORIONIS OBJECTS

R. Millan-Gabet,[1] J. D. Monnier,[2] R. L. Akeson,[1] L. Hartmann,[3] J.-P. Berger,[4] A. Tannirkulam,[2] S. Melnikov,[5] R. Billmeier,[2] N. Calvet,[3] P. D'Alessio,[6] L. A. Hillenbrand,[7] M. Kuchner,[8] W. A. Traub,[3] P. G. Tuthill,[9] C. Beichman,[1] A. Boden,[1] A. Booth,[10] M. Colavita,[10] M. Creech-Eakman,[10] J. Gathright,[11] M. Hrynevych,[11] C. Koresko,[1] D. Le Mignant,[11] R. Ligon,[10] B. Mennesson,[10] C. Neyman,[11] A. Sargent,[7] M. Shao,[10] M. Swain,[4] R. Thompson,[1] S. Unwin,[10] G. van Belle[1] G. Vasisht,[10] and P. Wizinowich[11]

Received 2005 July 11; accepted 2005 December 7

ABSTRACT

We present new *K*-band long-baseline interferometer observations of three young stellar objects of the FU Orionis class, namely, V1057 Cyg, V1515 Cyg, and Z CMa–SE, obtained at the Keck Interferometer during its commissioning science period. The interferometer clearly resolves the source of near-infrared emission in all three objects. Using simple geometric models, we derive size scales (0.5–4.5 AU) for this emission. All three objects appear significantly more resolved than expected from simple models of accretion disks tuned to fit the broadband optical and infrared spectrophotometry. We explore variations in the key parameters that are able to lower the predicted visibility amplitudes to the measured levels and conclude that accretion disks alone do not reproduce the spectral energy distributions and *K*-band visibilities simultaneously. We conclude that either disk models are inadequate to describe the near-infrared emission or additional source components are needed. We hypothesize that large-scale emission (tens of AU) in the interferometer field of view is responsible for the surprisingly low visibilities. This emission may arise in scattering by large envelopes believed to surround these objects.

Subject headings: infrared: stars — instrumentation: interferometers — planetary systems: protoplanetary disks — stars: formation — stars: individual (V1057 Cygnus, V1515 Cygnus, Z Canis Majoris) — techniques: high angular resolution

1. INTRODUCTION

FU Orionis objects are a small but remarkable class of stars that display several-magnitude outbursts in visible light, followed by decade-long fading phases. They also exhibit fluxes in excess of photospheric levels at infrared wavelengths, broad and doubled spectral absorption lines, and wavelength-dependent rotational velocities. Two main theories compete to explain their nature. Herbig et al. (2003 and references therein) favor a model in which the flare occurs in an unstable star rotating near breakup and where the spectral properties are explained by a rapidly rotating G supergiant photosphere overlaid with a rising cooler shell. In contrast, a more widely accepted view first proposed by Hartmann & Kenyon (1985) is that FU Orionis stars are pre–main-sequence objects and that all the observables have their origin in Keplerian circumstellar disks and prenatal infalling envelopes that surround them (see also Hartmann et al. [2004] for recent arguments in relation to the disk vs. rapidly rotating star debate). In this picture, the outbursts have their origin in sudden increases in the accretion rate through the disk, and all young stars may experience (probably recurrent) FU Orionis phases during their evolution (see also the review by Hartmann & Kenyon 1996).

Although the existence of circumstellar disks around young stars is well established observationally, very little is directly known about the structure and properties of the innermost disk regions ($\lesssim$1 AU). For solar-mass and intermediate-mass young stars, disk models have been reasonably successful at reproducing the infrared flux excesses characteristic of these systems, as well as the spectroscopic signatures of the accretion process itself. However, these efforts are fundamentally limited by the fact that the observations are spatially unresolved, which introduces important degeneracies with respect to the spatial distribution of the emitting material.

The degeneracies with respect to the spatial distribution of material inherent in spatially unresolved observations can be lifted by observations using a long-baseline interferometer, and important progress has already been made using this technique. For Herbig Ae/Be and T Tauri objects (young stars of intermediate and solar-type mass, respectively) all observations to date have revealed surprisingly large spatial scales for the near-infrared (NIR) emission (Millan-Gabet et al. 1999; Tuthill et al. 1999; Akeson et al. 2000, 2002, 2005a, 2005b; Millan-Gabet et al. 2001; Eisner et al. 2004, 2005; Monnier et al. 2005), prompting in part a significant revision of disk models, whereby previously ignored detailed physics of the disk inner edge are now incorporated with some success (Natta et al. 2001; Dullemond et al. 2001; Monnier & Millan-Gabet 2002; Muzerolle et al. 2003; Vinković et al. 2003). For a review of observational breakthroughs in this area recently made possible by interferometric

[1] Michelson Science Center, California Institute of Technology, Mail Stop 100-22, Pasadena, CA 91125; rafael@ipac.caltech.edu.
[2] Department of Astronomy, University of Michigan, Ann Arbor, MI 48109-1090.
[3] Harvard-Smithsonian Center for Astrophysics, Cambridge, MA 02138.
[4] Laboratoire d'Astrophysique de Grenoble, 414 rue de la Piscine, 38400 Saint Martin d'Heres, France.
[5] Ulugh Beg Astronomical Institute, Tashkent 700052, Uzbekistan.
[6] Universidad Nacional Autónoma de México.
[7] Department of Astronomy, California Institute of Technology, Pasadena, CA.
[8] Princeton University, Princeton, NJ.
[9] Department of Physics, University of Sydney.
[10] Jet Propulsion Laboratory, California Institute of Technology, Pasadena, CA 91109.
[11] W. M. Keck Observatory, California Association for Research in Astronomy, Kamuela, HI 96743.

TABLE 1
Basic Properties of Targets

Name	R.A. (J2000.0)	Decl. (J2000.0)	V[a] (mag)	J[a] (mag)	H[a] (mag)	K[a] (mag)	d (pc)	Adopted $T_\star$[b] (K)	SED Photometry References[c]
V1057 Cyg.....	20 58 53.7	+44 15 28.4	11.7	8.0	7.0	6.2	550 ± 100[d]	6200	1, 2, 3, 4
V1515 Cyg.....	20 23 47.6	+42 12 24	12.4	8.9	8.0	7.4	1000 ± 200[e]	5845	2, 4, 5
Z CMa–SE.....	07 03 43.2	−11 33 06.2	9.8	6.5	5.2	3.8	1150[f]	6360	2, 4, 6, 7

Note.—Units of right ascension are hours, minutes, and seconds, and units of declination are degrees, arcminutes, and arcseconds.

[a] As discussed in the text, these objects are by definition highly variable. The V and infrared magnitudes in this table are from SIMBAD and 2MASS, respectively, and are intended to be merely representative. See the text and references in this table for a description of how the SEDs used in the data analysis have been constructed. For Z CMa the magnitudes given in this table are for the total system.

[b] The true photospheric spectral types are not known; as there are no preoutburst spectra of these objects, these values are typical of what is quoted in the literature. The exact photospheric effective temperatures are, however, inconsequential to the analysis given the negligible stellar flux contribution in the models considered.

[c] As indicated in the text, we use near-contemporaneous *UBVR* photometry obtained at Maidanak Observatory (ROTOR program). In this column we provide the relevant references for additional literature photometry used to construct our SEDs.

[d] Straizys et al. (1989).

[e] Racine (1968).

[f] Herbst et al. (1978).

References.—(1) Kopatskaya et al. 2002; (2) 2MASS All-Sky Point Source Catalog; (3) Ábrahám et al. 2004; (4) van den Ancker et al. 2004; (5) Kenyon et al. 1991; (6) Millan-Gabet & Monnier 2002; (7) Koresko et al. 1991.

techniques at infrared wavelengths, the reader is referred to Millan-Gabet et al. (2006).

For FU Orionis objects, far fewer direct observational constraints exist at those scales. On the other hand, following the initial outburst the disk emission in FU Orionis objects outshines that of their central stars by many orders of magnitude, making them in principle ideal laboratories for testing theories describing the structure and physical properties of accretion disks. Indeed, the interpretation is freed from several complicating factors that affect the more evolved Herbig Ae/Be and T Tauri systems: instead of having multiple source components (star plus disk) and disk-heating mechanisms (stellar irradiation plus active accretion), only the disk component and active accretion matter for interpreting observations of FU Orionis objects. Given that these same theories are being applied to the disks inferred to exist around all young stars and that the physical conditions in the inner parts of those disks set the initial conditions for planet formation, it is important to validate the disk paradigm using FU Orionis objects as ground truth tests. The very first young stellar object to be resolved by long-baseline optical interferometry was in fact FU Orionis itself, and in their original analysis and follow-up work Malbet et al. (1998, 2005) concluded that the visibility amplitudes measured agreed well with those predicted by thermal emission in an accretion disk with the canonical temperature profile $T \sim r^{-3/4}$ with parameters tuned to fit the spectral energy distribution (SED).

In this paper we present new interferometer data on three other well-known FU Orionis objects and find instead that the NIR emission is overresolved relative to predictions of models that consist only of a standard disk emitting thermally. In § 2 we present the observations, instrumental arrangement, and data analysis; in § 3.1 we derive spatial scales for the NIR emission using simple geometric models of general applicability; in § 3.3 we construct accretion disk models with which we attempt to simultaneously fit the broadband SEDs and visibility amplitude data; in § 3.4 we consider additional source components that may be required in order to explain the measured visibilities; and in § 4 we discuss our results in the broader context and suggest future lines of investigation.

2. OBSERVATIONS AND DATA ANALYSIS

We have observed three well-studied FU Orionis objects: V1057 Cyg, V1515 Cyg, and the southeast component of the binary system Z CMa. Basic properties of these objects are given in Table 1. We note that the photometry data given in this table are meant to inform about the instrumental conditions only; photometry used for modeling was constructed as described in § 3.2.

These observations were made at the Keck Interferometer (KI) during its visibility science commissioning period (2002–2004). The KI (Colavita et al. 2004) consists of the two 10 m aperture Keck telescopes, separated by 85 m along a direction $\sim 38^\circ$ east of north, corresponding to a minimum fringe spacing of 5.3 milliarcseconds (mas) at 2.2 μm. In order to coherently combine the NIR light from such large apertures, each telescope uses a natural guide star adaptive optics (AO) system (Wizinowich et al. 2003). Optical delay lines correct for sidereal motion, and the telescope beams are combined at a beam splitter before the light is focused onto single-mode (fluoride) fibers, which impose a $\sim$50 mas (FWHM) field of view (FOV) for all data reported herein. While both H- and K-band observations are now possible, only broad K-band (2.18 μm, $\Delta\lambda = 0.3$ μm) data are reported here. For the four nights over which the data presented here were taken, observing conditions could be characterized as average, with fringe phase noise ("jitter," a measure of atmospheric seeing + instrument noise) in the range 0.5–1.25 rad and constant for calibrators and targets. The system visibility, observed on calibrator point sources, was always normal ($V^2_{\rm syst} = 0.6$–0.7).

We note that, although the angular separation of the components in the Z CMa system is only $\sim 0\farcs1$ (Koresko et al. 1991), the AO subsystems at KI clearly resolve the system, such that either binary component can be selected for interferometer measurements. Therefore, for the data presented here, the instrument has isolated the contribution from the southeast component, believed to be a FU Orionis object (Hartmann et al. 1989; Koresko et al. 1991). The northwest component is believed to be a high-mass young star surrounded by a dusty envelope (see, e.g., Garcia et al. 1999) and was also resolved by KI; these results are discussed in Monnier et al. (2005). With this method, given the relatively small angular distance between the two components, it is important to be sure that the fringe detector (1) was pointed at the intended component and (2) received no extra flux from the other one. We have performed several checks to verify this. First, the mean K-band fluxes measured from each component are in a ratio (the Herbig component being $\sim$3 times

TABLE 2
Calibrator Star Information

Name	V	J	K	Spectral Type	UD Diameter (mas)
HD 199178	7.2	5.7	5.2	G2 V	0.44 ± 0.07
HD 192985	5.8	5.0	4.8	F5 V	0.43 ± 0.06
HIP 102667.....	8.8	6.4	5.5	K2 V	0.49 ± 0.16
HD 227049	9.1	7.0	6.3	K2 III	0.30 ± 0.10
HD 332518	9.2	6.9	6.2	K5 V	0.38 ± 0.08
HD 52919	8.3	6.4	5.7	K5 V	0.42 ± 0.09
HD 48286	7.1	5.9	5.5	F7 V	0.35 ± 0.08
HD 60491	8.2	6.5	6.0	K2 V	0.33 ± 0.05

brighter than the FU Orionis component) that approximately agrees with (variable) values found in the literature (see references above). Second, we have verified that the fringes for each component were found at different optical delays, which differ by amounts consistent with the $\sim 0\farcs1$ astrometric offset. Finally, the single-mode fibers, which feed the fringe camera, impose a FOV ($\sim$50 mas as mentioned above) with an approximately Gaussian tapering. Therefore, even assuming a 3 times higher flux on the (off axis) Herbig component, its flux contribution to the on-axis beam is less than 1%, contributing negligibly to the measured visibilities. Moreover, the single-beam fluxes fluctuate by 30% or less, very consistently for all objects (the Z CMa components and the three calibrators used), indicating that uncompensated tip-tilt angle fluctuations are much less than 1 FWHM and again implying a small fraction of flux contamination by Z CMa–NW to the Z CMa–SE measurement.

The square of the fringe visibility (V^2) was measured using the ABCD method (using a dither mirror; see also Shao & Staelin 1977), and we followed well-tested strategies described for the Palomar Testbed Interferometer (PTI; Colavita 1999), except that corrections for unbalanced telescope fluxes were improved and jitter corrections were not applied. These forms of jitter corrections are relevant when optical path fluctuations are dominated by atmospheric residuals outside the fringe tracker bandwidth. At KI, these fluctuations are dominated by air motions in the Coudé path and do not obey the same statistics, and detailed tests have shown that standard jitter corrections do not improve the data calibration. Calibration of fringe data was performed by interspersing target observations with those of unresolved calibrators; basic information on the calibrator stars used is given in Table 2. We note that although the calibrator stars are significantly brighter than the target FU Orionis objects at visual wavelengths where the AO correction is performed, calibration tests (described in Akeson et al. 2005b) have shown that no systematic effects are introduced. Further details on the data reduction and calibration procedures may be found in Colavita et al. (2003) and Swain (2003).[12]

The calibrated V^2 results appear in Table 3, along with the projected baseline (u and v), date of each observation, and calibrator information. The V^2 errors reported in Table 3 only include statistical errors. Internal data quality checks have established a conservative upper limit to the systematic error $\Delta V^2 = 0.05$, which we add in quadrature and include in all model fitting (and figures) presented in this paper.

3. RESULTS

3.1. *Characteristic Sizes of the Near-Infrared Emission*

As can been seen in Table 3, all three sources are clearly resolved by the KI (calibrated $V^2 < 1.0$). Since the complex visibility is related to the source brightness by a Fourier transform relation (see, e.g., Goodman 1985), we can use a simple a priori representation of the object morphology and fit to the measured visibility amplitudes in order to extract source parameters of astrophysical value. This approach has the merit of providing fundamental new information about the NIR emission (size scale) that is independent of (often poorly constrained) details of specific physical models.

We use two plausible geometric representations for the NIR brightness: a Gaussian and a uniform ring. The parameters to be fit are the Gaussian full width at half-maximum (FWHM) and the ring diameter, respectively (the ring thickness is poorly constrained by measurements in the first lobe of the visibility function, and following previous work [e.g., Monnier et al. 2005], we adopt a 20% fractional ring width). These results are given in Table 4. We note that in our sample, the only object previously resolved at these scales is V1057 Cyg, for which Wilkin & Akeson (2003) similarly derive a Gaussian diameter that is larger than ours but within errors. In §§ 3.2 and 3.3 we test the detailed predictions of accretion disk models against both our new visibility measurements and reconstructed broadband SEDs.

3.2. *Constructing the SEDs*

It is not the purpose of this paper to perform detailed SED modeling, nor do our main conclusions depend on it. However, since FU Orionis objects are by definition photometrically variable, we have taken some care to construct meaningful (i.e., as

[12] As well as in a series of technical memos at the Michelson Science Center (http://msc.caltech.edu/KISupport).

TABLE 3
Calibrated Visibility Amplitude Data

Name	UT Date	Julian Date	u (m)	v (m)	V^2	Calibrators
V1057 Cyg.....	2002 Jun 27	2,452,453	44.519	67.770	0.727 ± 0.161	HD 199178, HD 192985, HIP 102667
	2002 Oct 24	2,452,572	43.427	70.711	0.791 ± 0.093	HD 199178, HD 199998
V1515 Cyg.....	2003 May 21	2,452,781	54.973	55.878	0.840 ± 0.030	HD 227049, HD 332518
	2003 May 21	2,452,781	53.245	59.776	0.725 ± 0.087	HD 227049, HD 332518
	2003 May 21	2,452,781	51.096	63.262	0.707 ± 0.065	HD 227049, HD 332518
Z CMa–SE.....	2004 Apr 3	2,453,099	24.195	51.929	0.158 ± 0.016	HD 48286, HD 52919, HD 60491
	2004 Apr 3	2,453,099	23.753	51.887	0.177 ± 0.009	HD 48286, HD 52919, HD 60491

Note.—This table shows only the statistical V^2 error, as discussed in § 2; an additional systematic error of 0.05 is added (in quadrature) to all data for fitting purposes, and the total error also is shown in all figures.

TABLE 4
Characteristic Near-Infrared Sizes

Name	Gaussian FWHM (mas)	Gaussian FWHM (AU)	Ring Inner Diameter (mas)	Ring Inner Diameter (AU)
V1057 Cyg.....	1.04 ± 0.23	0.57 ± 0.16	1.11 ± 0.24	0.55 ± 0.15
V1515 Cyg.....	1.05 ± 0.12	1.05 ± 0.24	1.13 ± 0.12	1.13 ± 0.20
Z CMa–SE.....	3.94 ± 0.24	4.53 ± 0.48	3.81 ± 0.18	4.38 ± 0.21

near-contemporaneous as possible) SEDs from existing data, as follows:

V1057 Cyg.—We use near-contemporaneous *UBVR* data provided by one of us (S. M.) and obtained in 2002 July and August at the Maidanak High Altitude Observatory as part of a long-term monitoring campaign of young stars (the ROTOR project; Herbst & Shevchenko 1999; Clarke et al. 2005). *I*-band data are interpolated between Kopatskaya et al. (2002) and photometry obtained by one of us (A. T.) at the MDM observatory in 2004 November–December. The NIR *JHK* photometry is from the Two Micron All Sky Survey (2MASS). Ábrahám et al. (2004) show a factor of 2 fading at NIR wavelengths between 1983 and 1996; assuming a constant rate of fading, this represents only a 0.08 mag fading between the 2MASS (2000 June) and KI epochs (2002 June and October), unimportant for our purposes. We nevertheless augment the 2MASS errors by 0.1 mag to allow for this level of variation, as well as the flickering known to exist in similar systems (see, e.g., van den Ancker et al. 2004; Kenyon et al. 2000). Thermal-IR data are from ISOPHOT as presented by Ábrahám et al. (2004).

V1515 Cyg.—Same as above, except that (1) no *I*-band data is available and (2) given the large ISOPHOT beam and beam confusion issues discussed for this object by Ábrahám et al. (2004), we use long-wavelength fluxes from the aperture photometry in Kenyon et al. (1991). We note that the level of NIR fading reported by Ábrahám et al. (2004) is much less significant even than for V1057 Cyg. The epoch of Maidanak *UBVR* data is 2003 June; the epoch of *JHK* 2MASS data is 1998 November.

Z CMa–SE.—Composing an SED for the FU Orionis component in this system is further complicated by the fact that most existing photometry is for the total system. For *UBV* we use the near-contemporaneous Maidanak photometry (epoch 2004 January), given that at these wavelengths the FU Orionis component is thought to dominate the total flux (see, e.g., Thiebaut et al. 1995). An estimate of the *R*-band flux is obtained from the Maidanak photometry using the flux ratio of Thiebaut et al. (1995). Infrared *J* and *H* fluxes are estimated by combining the 2MASS total fluxes (epoch 1998 December) and the flux ratios from the spatially resolved observations of Millan-Gabet & Monnier (2002; epoch 2001 January). At longer wavelengths, the infrared fluxes are from the discovery observations of Koresko et al. (1991; epoch 1990 November). The *K*-band flux has been dimmed by 0.2 mag in order to account for the fading observed by van den Ancker et al. (2004).

3.3. *Accretion Disk Models*

Accretion disk models have proved successful at reproducing many of the observational properties of FU Orionis objects (Hartmann & Kenyon 1985, 1996 and references therein). A key prediction of accretion disk models is the shape of the broadband SEDs, and agreement with observations provides one of the strongest lines of support for the disk hypothesis. For a steady Keplerian disk that is optically thick and geometrically thin, its radial temperature profile can be parameterized as $T(r) = T_{\max}(r/R_\star)^{q=-3/4}[1 - (R_\star/r)^{1/2}]^{1/4}$ for $r > 1.36R_\star$ and as $T(r) = T_{\max}$ between this radius and the stellar surface (Shakura & Sunyaev 1973; Lynden-Bell & Pringle 1974). The maximum temperature in the disk ($T_{\max}$) is related to the stellar mass and disk accretion rate, and good SED fits are obtained with relatively high values of this parameter (∼5000–7000 K), together with stellar radii normal for low-mass young stars (2–4 $R_\odot$). Under these conditions, the disk flux far outshines the central star[13] at all wavelengths, and the model has relatively few parameters. If the disk inclination can be reasonably well constrained by other means, then the extinction A_V, stellar radius $R_\star$, and maximum disk temperature $T_{\max}$ are all well constrained by the shape and level of the SED. Once a model solution is thus obtained, the corresponding visibilities can be computed, and a straightforward comparison to the KI data can be made.

Another characteristic of these single-power-law models is that, except for inclination effects (believed to be low for our sources; e.g., Kenyon et al. 1988), flux and "size" at a given wavelength are simply related. This scaling and comparison with the FU Orionis PTI observations of Malbet et al. (1998) immediately reveal that our targets are overresolved with respect to expectations from the disk model. Indeed, our observations of V1057 Cyg and V1515 Cyg are approximately consistent with the visibility curve for FU Orionis in Malbet et al. (1998), corresponding to a disk solution that also fits its SED. However, V1057 Cyg and V1515 Cyg are ∼38 and 8 times *fainter* than FU Orionis, respectively. Therefore, a disk model that fits the SEDs of V1057 Cyg and V1515 Cyg will clearly underestimate their visibilities.

Following previous workers, our disk is represented by a series of concentric annuli. At each radius, the annulus radiates as a Kurucz supergiant photosphere (Kurucz 1979) of effective temperature equal to the disk temperature at that radius, unless the temperature is lower than 3500 K, in which case we use blackbody emission. We use solar metallicity and a value of the surface gravity appropriate for the temperature at each radius. Model SEDs are reddened using the law of Mathis (1990), using a total-to-selective extinction ratio $R_V = 3.1$. The KI data were obtained essentially at a single baseline position angle and therefore cannot constrain the disk inclination. Moreover, for V1057 Cyg and V1515 Cyg the rotational velocities measured from line broadening are relatively low, such that unless the stars have unreasonably low mass, the inclinations must be low ($i < 30^\circ$; Kenyon et al. 1988). Therefore, we consider mainly face-on disks in our fits, but explore the effects of disk inclination.

The solutions found from fitting the SEDs are similar to those found by previous workers and are shown in Table 5. The data and disk models are shown in Figure 1. For V1057 Cyg, in this and subsequent visibility figures, we include (*open circle*) the data obtained at the PTI by Wilkin & Akeson (2003). However,

[13] We note that SED solutions with much lower $T_{\max}$ and larger $R_\star$ are possible, but require essentially all the $U \rightarrow R$ flux to arise in the stellar photosphere, which is in conflict with the measured line profiles.

TABLE 5
Model Parameters

Name	Flat Disk				Flared Disk		Minimum Incoherent Fluxes	
	q	T_{max} (K)	$R_\star/R_\odot$	A_V	q_2	$r_0/R_\star$	f_i ($V_c = 1.0$) (%)	f_i ($V_c = V_{disk}$) (%)
V1057 Cyg.....	−0.75	7280 ± 191	2.4 ± 0.1	4.2	−0.45	100	12 ± 5	9 ± 5
V1515 Cyg.....	−0.75	8014 ± 280	2.1 ± 0.2	3.0	−0.45	100	10 ± 2	9 ± 2
Z CMa–SE.....	−0.75	5785 ± 351	7.7 ± 0.6	1.9	...	...	59 ± 3	58 ± 3

due to the very different FOVs of the KI and PTI instruments and given the possible effect of large-scale emission in these objects (see § 3.4), we choose not to include this datum in our fitting exercises. In the visibility panels it can be clearly seen that geometrically flat accretion disks (i.e., single power law with $q = -0.75$) significantly overestimate the visibility amplitudes at K band, because the relatively steep temperature profile results in the NIR emission coming from regions of the disk that have radii too small

As is well known and as is also apparent from the SED panels of Figure 1, for some FU Orionis objects (such as V1057 Cyg and V1515 Cyg) longward of ~10 μm the infrared fluxes far exceed the flat-disk predictions. Flared disks having a flatter temperature profile have been proposed as one solution to explain the long-wavelength SED (see, e.g., Kenyon & Hartmann 1991; Lachaume 2004). We have approximated this model by specifying a double power law for the temperature profile in the disk. Following Kenyon & Hartmann (1991), we use Figure 4 of their paper and select the case of most extreme flaring [$H_0 = 0.2$; this parameter determines the disk height profile as a function of radius, $H_d(r)/R_\star = H_0(r/R_\star)^{9/8}$] to approximate their detailed temperature profile with two slopes: $q = -0.75$ for $r < 100R_\star$ and $q_2 = -0.45$ outside this radius. Figure 1 shows that for flared disks the long-wavelength SED is now

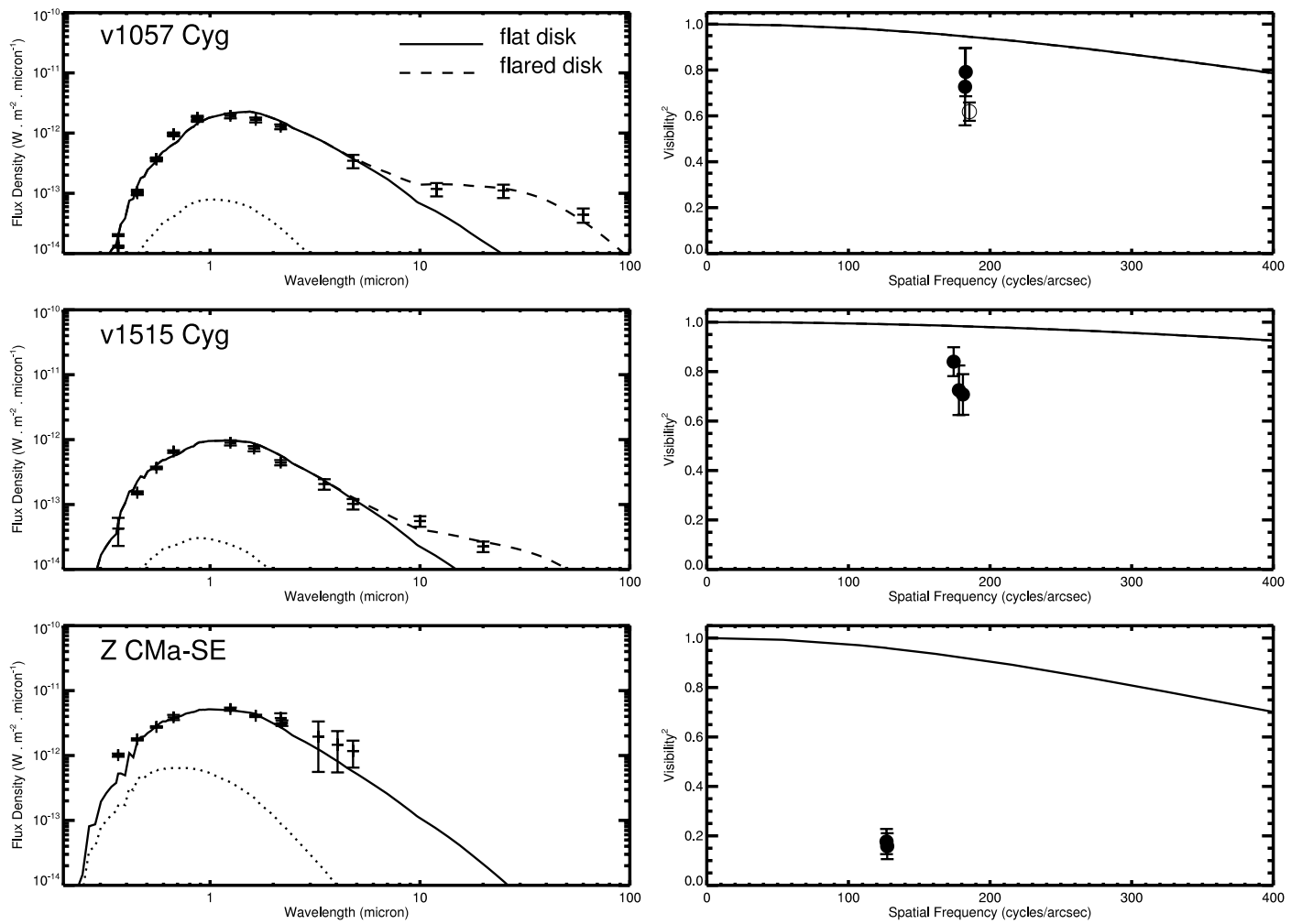

Fig. 1.—Data and disk model results. *Left*, SED; *right*, visibility amplitudes. For V1057 Cyg we include the visibility data obtained at the PTI by Wilkin & Akeson (2003; *open circle*). The models correspond to best SED fits and are calculated for the parameters of Table 5. The solid line shows the model for a flat disk; the dashed line shows the model for a flared disk. For the flat-disk model, the fitting procedure uses only SED data with $\lambda < 10$ μm, while fitting the flared-disk model uses the whole SED. In the visibility panels the two lines overlap because the flared-disk regions do not contribute significant K-band flux. The dotted line in the SED panels is the stellar photosphere. For Z CMa–SE, we consider only the flat-disk model, given the lack of resolved long-wavelength photometry.

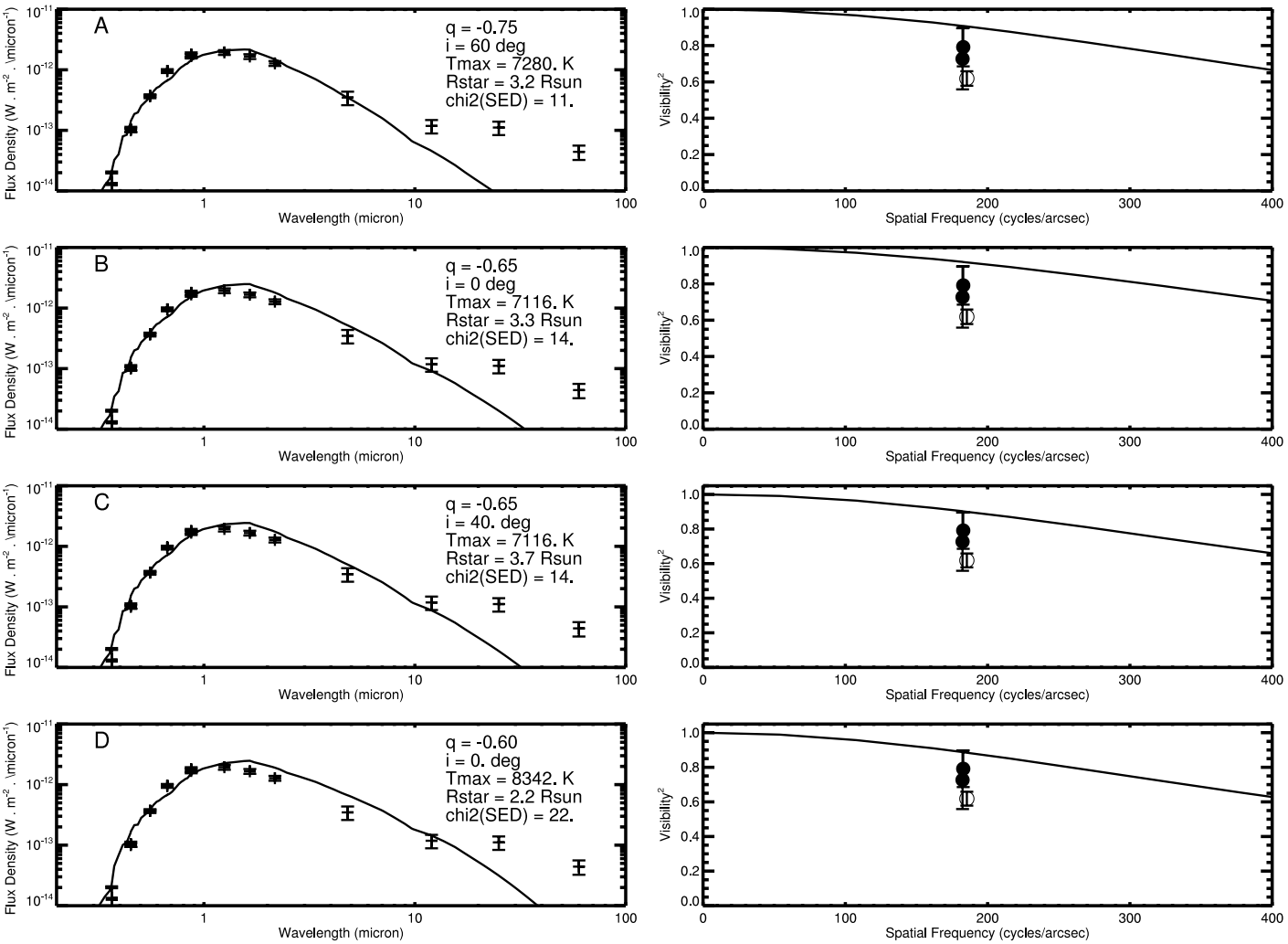

FIG. 2.—V1057 Cyg. (*a*) Effect of disk inclination; (*b–d*) different values of the temperature radial exponent for the inner disk. These models may be compared with the V1057 Cyg best fit (zero inclination) of Fig. 1, for which we have the reference reduced $\chi^2_{\rm SED} = 11$. (*a*) Although a 60° inclination reproduces the SED equally well, it is the minimum inclination required to just become consistent with the upper limit of the V^2 data. (*b*) The value $q = -0.65$ produces a marginally acceptable SED fit, but is not sufficient to touch the V^2 upper bound. (*c*) Also for $q = -0.65$. Additionally including inclination can reproduce the V^2 upper bound, but a relatively large value of 40° is required. (*d*) The value $q = -0.6$ reproduces the V^2 upper bound, even for zero inclination, but results in a significantly poorer SED fit. In all cases, SED data longward of 10 μm, although plotted, is not included in the calculation of the $\chi^2_{\rm SED}$, since here we only attempt to model the inner disk regions where the *K*-band flux arises. For V1057 Cyg we include the visibility data obtained at the PTI by Wilkin & Akeson (2003; *open circle*).

well reproduced; however, the *K*-band visibilities are indistinguishable from the nonflared case, simply because the flared-disk regions are too cool to thermally emit significant NIR radiation.

For Z CMa–SE, there exists no resolved long-wavelength photometry, and therefore we consider only the flat-disk model. This source is much more resolved than the other two, at levels very difficult to explain with thermal disk emission only.

We have explored two additional possibilities to attempt to explain the low visibilities measured by KI using purely thermal disk emission: disk inclination and a nonstandard temperature profile ($q \neq -0.75$) for the inner disk, as follows. The SEDs can be well fit for nonzero inclinations, provided the flux lost to surface area is recovered by increasing $R_\star$, which also has the desired effect of resulting in lower visibilities (a larger NIR source) if the KI baseline position angle also happens to be aligned with the long dimension of the elliptical brightness. However, we find that, even allowing for the most favorable disk orientation, the inclinations needed to match the KI data are very large, $i \sim 60°–85°$, well outside the upper limit inferred from line broadening for the mass range of typical young stars, as mentioned above. We illustrate this difficulty for V1057 Cyg in Figure 2*a*, and similar conclusions apply to V1515 Cyg.

Relaxing the assumption that $q = -3/4$ and allowing a flatter profile in the inner disk would also result in larger NIR emission regions. Exploring this departure from the canonical temperature profile exponent is a reasonable approach, given that (1) the decaying and flickering light curves show that the disk is not exactly steady state and (2) the absence of the expected boundary layer emission (Kenyon & Hartmann 1989) calls into question the radial temperature profile near the inner disk edge. We find, however, that matching the visibilities would require $q \geq -0.6$, and for such exponents the SED cannot be satisfactorily fit, because of the sensitivity of its infrared slope to the temperature profile exponent. Allowing a free *q*-parameter *and* the disk to be inclined does not provide a satisfactory solution either, simply because $q \sim -0.65$ is the flattest exponent allowed by the NIR SED slope, and for such exponents large disk inclinations would again be needed to match the visibilities. We illustrate these difficulties for V1057 Cyg in the bottom three panels of Figure 2*b–2d*, and similar conclusions apply to V1515 Cyg.

Finally, we note that allowing the disk inner radius to be a free parameter ($r_{\rm inner} \gg R_\star$) can formally result in acceptable simultaneous fits to the SEDs and visibilities, but we believe these are not physically viable for our targets (contrary to the case of Herbig Ae/Be and T Tauri systems). Allowing an inner disk radius several times larger than $R_\star$ (for example, $10R_\star$ for V1057 Cyg) and keeping the same $T_{\rm max}$ to preserve the SED shape result in NIR emission originating at larger radii (comparable to the ring radii of § 3.1) and lower visibilities, in agreement with the observations. However, to preserve the SED flux levels, the disk needs to be inclined by very large amounts (86° for V1057 Cyg), in contradiction to the limits derived by Kenyon et al. (1988). Moreover, physical disk models (Clarke et al. 1990; Hartmann et al. 1993; Bell & Lin 1994) indicate that for the high accretion rates of FU Orionis systems, it is very implausible that a central optically thin disk region could exist, and the emission lines that would be expected if it did are not observed.

3.4. *Additional Model Components*

The difficulties encountered in § 3.3 previous section in using standard disk models to simultaneously reproduce the observed SEDs and visibilities may indicate that these models are inadequate for describing the NIR emission. Alternatively, additional source components could exist that are responsible for the low measured visibilities.

3.4.1. *Extended Structure*

A possible explanation is that the measured visibilities are not entirely due to compact NIR thermal emission in a flat or flared disk, but that a small but nonnegligible fraction of the total flux arises in larger scale structure within the 50 mas FOV of the interferometer (25 and 50 AU at $d = 500$ and 1000 pc, respectively). The size of this region and the flux it contributes are degenerate when modeling its contribution to the visibility. However, a *minimum* flux can be inferred if we assume that it is completely incoherent (i.e., completely resolved by the interferometer), which for the spatial frequencies sampled and the distances to the three objects corresponds to size scales $\gtrsim$4, 5, and 10 AU, for V1057 Cyg, V1515 Cyg, and Z CMa–SE, respectively. The needed amount of incoherent flux can be analytically estimated as follows. For an object consisting of a central compact object (the NIR disk; we neglect the stellar flux) plus an extended component the measured visibility (at a given spatial frequency) is $V_{\rm meas} = (F_c V_c + F_e V_e)/F_t$, where the subscripts in the flux (F) and visibility (V) of each component denote c = compact, e = extended, and t = total. In the case that the extended component is completely resolved, we have $V_e = 0.0$, and the minimum incoherent flux fraction is given by $f_i = F_e/F_t = 1.0 - V_{\rm meas}/V_c$. Table 5 summarizes the values for f_i obtained for the cases in which the compact object is unresolved ($V_c = 1.0$) and, more meaningfully, the case in which the compact object is the accretion disk considered in § 3.3 and is resolved at the data spatial frequencies by the amounts predicted by the best SED-fit models (Table 5; Fig. 1). The effect of this additional component on the visibility curves is shown in Figure 3, where the ranges of f_i shown correspond to the values needed to reproduce the weighted mean visibility measured and visibility data upper limits given the +1 σ errors.

3.4.2. *Physical Origin of the Extended Emission*

Given the low thermal temperatures expected for any circumstellar material located at the scales considered above, this additional emission would physically correspond to scattering of thermal disk K-band photons by circumstellar material (at least for V1057 Cyg and V1515 Cyg, the fraction of incoherent flux derived above for Z CMa–SE is prohibitively high for a scattering origin). Our observations do not directly constrain the precise nature of the putative incoherent flux source; a reasonable hypothesis is that scattering occurs in the upper atmosphere of the outer disk or in envelope material.

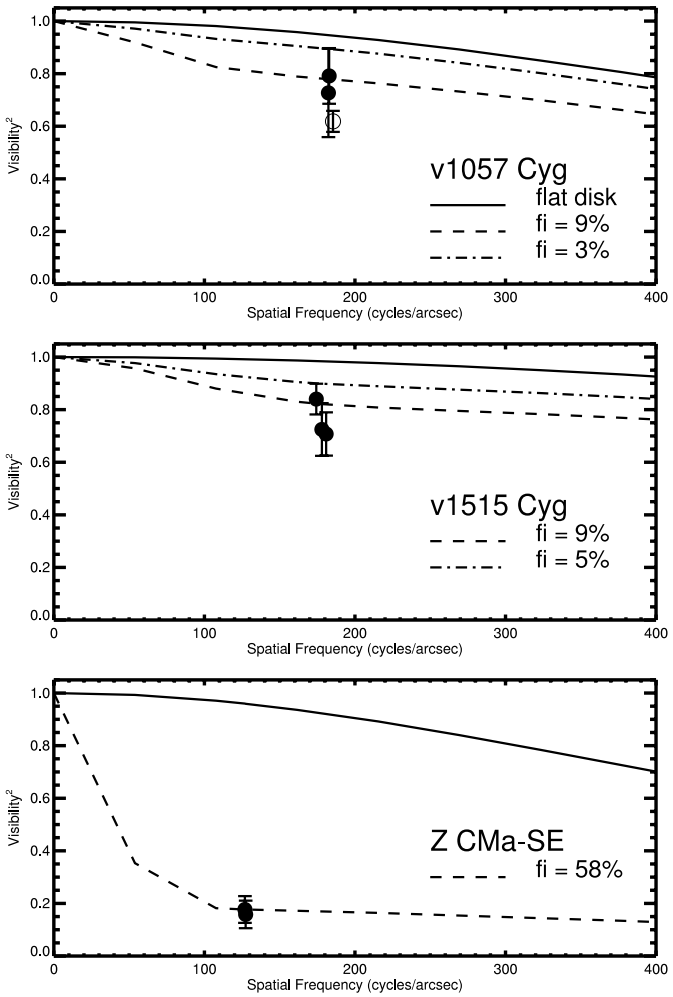

FIG. 3.—Adding incoherent fluxes to the best SED-fit disk models of Fig. 1 (*solid line*). The dashed and dash-dotted lines show how the visibilities are reduced to the desired levels by adding the indicated amounts of incoherent (completely resolved) flux to the disk models. The size of the region where this incoherent flux arises is not constrained by the observations, but for display it has been included in the model as a Gaussian component of FWHM equal to the minimum value that is completely resolved at the data spatial frequencies: 4, 4, and 10 AU for V1057 Cyg, V1515 Cyg, and Z CMa–SE, respectively. For V1057 Cyg we include the visibility data obtained at the PTI by Wilkin & Akeson (2003; *open circle*).

Kenyon & Hartmann (1991) first showed that thermal emission in infalling envelopes surrounding the V1057 Cyg and V1515 Cyg disks provides good fits to the long-wavelength excess fluxes in these systems. The putative envelopes have evacuated cones along the poles, cleared by bipolar outflows, which result in the relative unobscured views toward the central objects, as observed. Moreover, these authors favor the envelope hypothesis over flaring disks, due to the large degree of flaring that would be required to reproduce the long-wavelength SEDs, and the wavelength-dependent photometric decay curves. For T Tauri objects with flat SEDs, Natta (1993) has also proposed the existence of envelopes (tenuous in that case) that heat the outer disk regions by scattering stellar photons onto it.

The envelopes considered by Kenyon & Hartmann (1991) for V1057 Cyg and V1515 Cyg are characterized by $\sim$7 AU inner radii and temperatures at these radii of $\sim$few $\times$ 100 K, and it is therefore easy to see that adding such an envelope to the disk has no effect on the *K*-band visibilities if only thermal emission is considered; as pointed out by these authors, the emission below 10 μm and certainly at 2 μm is completely dominated by the disk. Moreover, the $\sim$7 AU inner radii imply that this component would indeed be completely resolved by the KI. Therefore, the basic considerations presented in § 3.4.1 provide the amounts of flux that the envelope would need to scatter at *K* band to reproduce the KI observations.

These are relatively large amounts of scattered *K*-band flux, originating in a relatively small FOV. However, building on the initial models of Kenyon & Hartmann (1991), more refined models of V1057 Cyg and V1515 Cyg are being explored and compared with new data from the Infrared Spectrograph on board the *Spitzer Space Telescope*, which involve infall to the disk at about 10 AU (J. Green et al. 2006, in preparation). Independent of model details, the long-wavelength excesses above what is expected for the disk are approximately 20% of the apparent total disk luminosity for V1057 Cyg and 12% of the total apparent luminosity of V1515 Cyg. If the effective scattering albedo of the envelope in the *K* band is of order of 0.5, then the envelopes invoked to explain the infrared excesses longward of $\sim$10 μm could be responsible for a scattered flux of 6%–10% within the FOV of the interferometer. This is in reasonable agreement with the observational requirements, given the uncertainties and likely complex geometry, implying that the scattering envelopes of V1057 Cyg and V1515 Cyg can in fact account for the *K*-band visibilities.

3.4.3. *Stellar Companion*

Dynamical interactions with a stellar companion have been invoked to explain the origin of the accretion rate outbursts in FU Orionis objects (Bonnell & Bastien 1992), and in fact several objects of the class are known to have "wide" (tenths of arcsec separations) companions. Motivated by the recent discovery of such a wide companion (separation $\sim$0.″5) to FU Orionis itself (Wang et al. 2004), Reipurth & Aspin (2004) propose that the FU Orionis phenomenon corresponds to the formation of binary systems by the breakup of small, nonhierarchical systems. For FU Orionis itself, this scenario predicts a third close companion, at separation $\sim$10 AU, perhaps corresponding to the interferometric signature detected by Malbet et al. (2005).

A binary system produces a sinusoidal visibility amplitude curve as a function of projected baseline, with period given by the (inverse of) angular separation and an amplitude given by the flux ratio between the two components. Given our limited data set (essentially a single spatial frequency was measured for each object) and the sinusoidal response, many values of the binary parameters (flux ratio and companion location) result in visibility functions that reproduce our measurements equally well, and therefore a fitting exercise is not very informative. However, for reference, interesting bounds on the family of possible solutions are as follows. The measured visibility values imply a *maximum* flux ratio between the binary components of about 20:1, 20:1, and 2.5:1 for V1057 Cyg, V1515 Cyg, and Z CMa–SE, respectively. For this maximum value of the flux ratio, the *minimum* angular separations are about 1.0, 1.0, and 1.7 mas for V1057 Cyg, V1515 Cyg, and Z CMa–SE, respectively. For equal-flux components, the minimum separations become 0.4, 0.4, and 1.3 mas for V1057 Cyg, V1515 Cyg, and Z CMa–SE, respectively. We note that for these estimates we have considered a binary model in which the "primary" component is again the partially resolved best SED-fit disk of § 3.3.

4. DISCUSSION AND CONCLUSIONS

We have presented new observations that spatially resolve the NIR emission of three FU Orionis objects on mas scales, a first for two of the objects (V1515 Cyg and Z CMa–SE). The spatial scales for NIR emission are surprisingly large compared to predictions of simple accretion disk models. This indicates that the accretion models require modification or that additional model components are required.

As is well known, the infrared SED slopes sensitively probe the radial temperature profile in the disk, and we have shown that while exponents $q = -0.6$ or flatter would be required to match the measured visibilities, these solutions are not able to maintain good agreement with the SED data. We note, however, that in this approach tests of the validity of small variations to the disk temperature profile are limited by the accuracy of the SED photometry adopted, and therefore follow-up studies should ideally be performed using contemporaneous photometry of uniform quality.

It is interesting to contrast our results with the case of the prototype for the class, FU Orionis, which has only modest long-wavelength fluxes in excess of thermal emission in a flat accretion disk and for which the NIR interferometer data do agree well with this model, according to Malbet et al. (1998, 2005). We note that this conclusion rests on the ability to incline the FU Orionis disk by a relatively large amount ($i \sim 50^\circ$–60°), which in this case does not imply unreasonably low stellar masses, given the measured rotational velocities (Kenyon et al. 1988).

Given the existing indications for dense envelopes around V1057 Cyg and V1515 Cyg, we hypothesize as a natural explanation for the low measured visibilities that scattering by material located on tens of AU scales adds incoherent flux in the interferometer FOV, diluting the visibilities from the relatively compact inner disk. We note that this mechanism may also explain the somewhat larger size (Gaussian FWHM $= 1.36 \pm 0.07$ mas) found for V1057 Cyg by Wilkin & Akeson (2003), since PTI has a 1″ FOV, 20^2 times larger than that of KI. A full calculation of FOV effects in specific scattering models is beyond the scope of this paper; we simply note that considering the PTI measurement alone, the minimum incoherent flux fraction becomes $f_i = 21\% \pm 5\%$.

An important consequence of this interpretation is that it compromises the notion of using FU Orionis objects as *straightforward* test cases of accretion disk theories, at least for most of the better known candidate targets. Indeed, if the disk is not isolated, multibaseline and multiwavelength interferometer observations must be used to better discriminate between competing models. In particular, the hypothesis that scattering is at the origin of the low visibilities measured is testable using measurements in different NIR bands: at shorter wavelengths, where scattering is more efficient (e.g., *J* or *H* bands), the characteristic sizes should be larger, while thermal disks predict the opposite trend of larger sizes at longer wavelengths (with a detailed dependence that probes the flatness of the temperature profile). These multiwavelength observations are already possible at existing interferometers (e.g., KI and the AMBER instrument on the VLTI; Petrov et al. 2000) or upcoming instruments (e.g., the MIRC combiner at CHARA; Monnier et al. 2004). For objects with evidence for dense envelopes, self-consistent radiative transfer codes that include scattering should also be used

in order to include this effect in both the SEDs and visibilities for realistic geometries and dust properties.

The exciting possibility that all three objects are instead resolved due to the presence of stellar companions, sometimes invoked to explain the outbursts themselves, is also testable with follow-up interferometer observations with improved spatial frequency coverage. Given the KI visibility calibration accuracy (which translates into a 100 : 1 maximum detectable binary contrast), the telltale and unambiguous sinusoidal signatures would be easily detected even for the most pessimistic values of the binary contrast derived above.

The authors wish to thank the all members of the Keck Interferometer development team (JPL, MSC, and WMKO), whose dedicated efforts made this "shared risk" commissioning science possible. We also thank Francis Wilkin for providing the PTI data for V1057 Cyg. This material is based on work supported by NASA under JPL contracts 1236050 and 1248252, issued through the Office of Space Science. Data presented herein were obtained at the W. M. Keck Observatory from telescope time allocated to the National Aeronautics and Space Administration through the agency's scientific partnership with the California Institute of Technology and the University of California. The observatory was made possible by the generous financial support of the W. M. Keck Foundation. This research has made use of the SIMBAD database, operated at CDS, Strasbourg, France. This publication makes use of data products from the Two Micron All Sky Survey (2MASS), which is a joint project of the University of Massachusetts and the Infrared Processing and Analysis Center/California Institute of Technology, funded by the National Aeronautics and Space Administration and the National Science Foundation. This work has made use of services produced by the Michelson Science Center at the California Institute of Technology. The authors wish to recognize and acknowledge the very significant cultural role and reverence that the summit of Mauna Kea has always had within the indigenous Hawaiian community. We are most fortunate to have the opportunity to conduct observations from this mountain.

REFERENCES

Ábrahám, P., Kóspál, Á., Csizmadia, S., Kun, M., Moór, A., & Prusti, T. 2004, A&A, 428, 89
Akeson, R. L., Ciardi, D. R., van Belle, G. T., & Creech-Eakman, M. J. 2002, ApJ, 566, 1124
Akeson, R. L., Ciardi, D. R., van Belle, G. T., Creech-Eakman, M. J., & Lada, E. A. 2000, ApJ, 543, 313
Akeson, R. L., et al. 2005a, ApJ, 622, 440
———. 2005b, ApJ, 635, 1173
Bell, K. R., & Lin, D. N. C. 1994, ApJ, 427, 987
Bonnell, I., & Bastien, P. 1992, ApJ, 401, L31
Clarke, C., Lodato, G., Melnikov, S. Y., & Ibrahimov, M. A. 2005, MNRAS, 361, 942
Clarke, C. J., Lin, D. N. C., & Pringle, J. E. 1990, MNRAS, 242, 439
Colavita, M. M. 1999, PASP, 111, 111
Colavita, M. M., Wizinowich, P. L., & Akeson, R. L. 2004, Proc. SPIE, 5491, 454
Colavita, M. M., et al. 2003, ApJ, 592, L83
Dullemond, C. P., Dominik, C., & Natta, A. 2001, ApJ, 560, 957
Eisner, J. A., Hillenbrand, L. A., White, R. J. Akeson, R. L., & Sargent, A. I. 2005, ApJ, 623, 952
Eisner, J. A., Lane, B. F., Hillenbrand, L. A., Akeson, R. L., & Sargent, A. I. 2004, ApJ, 613, 1049
Garcia, P. J. V., Thiebaut, E., & Bacon, R. 1999, A&A, 346, 892
Goodman, J. W. 1985, Statistical Optics (New York: Wiley)
Hartmann, L., Hinkle, K., & Calvet, N. 2004, ApJ, 609, 906
Hartmann, L., & Kenyon, S. J. 1985, ApJ, 299, 462
———. 1996, ARA&A, 34, 207
Hartmann, L., Kenyon, S. J., & Calvet, N. 1993, ApJ, 407, 219
Hartmann, L., Kenyon, S. J., Hewett, R., Edwards, S., Strom, K. M., Strom, S. E., & Stauffer, J. R. 1989, ApJ, 338, 1001
Herbig, G. H., Petrov, P. P., & Duemmler, R. 2003, ApJ, 595, 384
Herbst, W., Racine, R., & Warner, J. W. 1978, ApJ, 223, 471
Herbst, W., & Shevchenko, V. S. 1999, AJ, 118, 1043
Kenyon, S., & Hartmann, L. 1989, ApJ, 342, 1134
Kenyon, S. J., Hartmann, L., & Hewett, R. 1988, ApJ, 325, 231
Kenyon, S. J., & Hartmann, L. W. 1991, ApJ, 383, 664
Kenyon, S. J., Hartmann, L. W., & Kolotilov, E. A. 1991, PASP, 103, 1069
Kenyon, S. J., Kolotilov, E. A., Ibragimov, M. A., & Mattei, J. A. 2000, ApJ, 531, 1028
Kopatskaya, E. N., Grinin, V. P., Shakhovskoi, D. N., & Shulov, O. S. 2002, Astrophysics, 45, 143
Koresko, C. D., Beckwith, S. V. W., Ghez, A. M., Matthews, K., & Neugebauer, G. 1991, AJ, 102, 2073
Kurucz, R. L. 1979, ApJS, 40, 1
Lachaume, R. 2004, A&A, 422, 171
Lynden-Bell, D., & Pringle, J. E. 1974, MNRAS, 168, L603
Malbet, F., et al. 1998, ApJ, 507, L149
———. 2005, A&A, 437, 627
Mathis, J. S. 1990, ARA&A, 28, 37
Millan-Gabet, R., Malbet, F., Akeson, R., Leinert, C., Monnier, J. D., & Waters, R. 2006, in Protostars and Planets V, ed. B. Reipurth et al. (Tucson: Univ. Arizona Press), in press
Millan-Gabet, R., & Monnier, J. D. 2002, ApJ, 580, L167
Millan-Gabet, R., Schloerb, F. P., & Traub, W. A. 2001, ApJ, 546, 358
Millan-Gabet, R., Schloerb, F. P., Traub, W. A., Malbet, F., Berger, J. P., & Bregman, J. D. 1999, ApJ, 513, L131
Monnier, J. D., Berger, J.-P., Millan-Gabet, R., & Ten Brummelaar, T. A. 2004, Proc. SPIE, 5491, 1370
Monnier, J. D., & Millan-Gabet, R. 2002, ApJ, 579, 694
Monnier, J. D., et al. 2005, ApJ, 624, 832
Muzerolle, J., Calvet, N., Hartmann, L., & D'Alessio, P. 2003, ApJ, 597, L149
Natta, A. 1993, ApJ, 412, 761
Natta, A., Prusti, T., Neri, R., Wooden, D., Grinin, V. P., & Mannings, V. 2001, A&A, 371, 186
Petrov, R., et al. 2000, Proc. SPIE, 4006, 68
Racine, R. 1968, AJ, 73, 588
Reipurth, B., & Aspin, C. 2004, ApJ, 608, L65
Shakura, N. I., & Sunyaev, R. A. 1973, A&A, 24, 337
Shao, M., & Staelin, D. H. 1977, Opt. Soc. Am. J., 67, 81
Straizys, V., Meistas, E., Vansevicius, V., & Goldberg, E. P. 1989, A&A, 222, 82
Swain, M. 2003, ApJ, 596, L163
Thiebaut, E., Bouvier, J., Blazit, A., Bonneau, D., Foy, F.-C., & Foy, R. 1995, A&A, 303, 795
Tuthill, P. G., Monnier, J. D., & Danchi, W. C. 1999, Nature, 398, 487
van den Ancker, M. E., Blondel, P. F. C., Tjin A Djie, H. R. E., Grankin, K. N., Ezhkova, O. V., Shevchenko, V. S., Guenther, E., & Acke, B. 2004, MNRAS, 349, 1516
Vinković, D., Ivezic, Z., Miroshnichenko, A. S., & Elitzur, M. 2003, MNRAS, 346, 1151
Wang, H., Liu, C., Qiu, J., Deng, N., Goode, P. R., & Denker, C. 2004, ApJ, 601, L83
Wilkin, F. P., & Akeson, R. L. 2003, Ap&SS, 286, 145
Wizinowich, P. L., Le Mignant, D., Stomski, P. J., Jr., Acton, D. S., Contos, A. R., & Neyman, C. R. 2003, SPIE, 4839, 9